Hindawi
Adsorption Science & Technology
Volume 2021, Article ID 5597299, 10 pages
https://doi.org/10.1155/2021/5597299

Research Article

Adsorption of Mn^{2+} from Aqueous Solution Using Manganese Oxide-Coated Hollow Polymethylmethacrylate Microspheres (MHPM)

Dhiraj Dutta, Jyoti Prasad Borah, and Amrit Puzari

National Institute of Technology Nagaland, Chumukedima, Dimapur, 797 103 Nagaland, India

Correspondence should be addressed to Amrit Puzari; amritpuzari@nitnagaland.ac.in

Received 15 September 2020; Accepted 18 February 2021; Published 15 March 2021

Academic Editor: Susana Valencia

Copyright © 2021 Dhiraj Dutta et al. This is an open access article distributed under the Creative Commons Attribution License, which permits unrestricted use, distribution, and reproduction in any medium, provided the original work is properly cited.

Results of investigation on adsorption of Mn^{2+} from aqueous solution by manganese oxide-coated hollow polymethylmethacrylate microspheres (MHPM) are reported here. This is the first report on Mn-coated hollow polymer as a substitute for widely used materials like green sand or MN-coated sand. Hollow polymethylmethacrylate (HPM) was prepared by using a literature procedure. Manganese oxide (MnO) was coated on the surface of HPM (MHPM) by using the electroless plating technique. The HPM and MHPM were characterized by using optical microscopy (OM), scanning electron microscopy (SEM), Fourier-transform infrared spectroscopy (FTIR), X-ray diffraction (XRD), and thermogravimetric analysis (TGA). Optical and scanning micrographs were used to monitor the surface properties of the coated layer which revealed the presence of MnO on the surface of HPM. TGA showed the presence of 4-5% of MnO in MHPM. Adsorption isotherm studies were carried out as a function of pH, initial ion concentration, and contact time, to determine the adsorption efficiency for removal of Mn^{2+} from contaminated water by the synthesized MHPM. The isotherm results showed that the maximum adsorption capacity of MnO-coated HPM to remove manganese contaminants from water is 8.373 mg/g. The obtained R^2 values of Langmuir isotherm and Freundlich isotherm models were 1 and 0.87, respectively. Therefore, R^2 magnitude confirmed that the Langmuir model is best suited for Mn^{2+} adsorption by a monolayer of MHPM adsorbent. The material developed shows higher adsorption capacity even at a higher concentration of solute ions, which is not usually observed with similar materials of this kind. Overall findings indicate that MHPM is a very potential lightweight adsorbent for removal of Mn^{2+} from the aqueous solution because of its low density and high surface area.

1. Introduction

Heavy metal contamination of water bodies from improperly disposed industrial wastes is a serious environmental problem across the world. Manganese is one among those heavy metal contaminants and is used principally in the manufacture of iron and steel alloys [1]. Manganese dioxide and other manganese compounds are used in products such as batteries, glass, and fireworks. Potassium permanganate is used as an oxidant for cleaning, bleaching, and disinfection purposes (HSDB, 2001) [2]. Manganese green sands are used in water treatment plants. An organic manganese compound, methylcyclopentadienyl manganese tricarbonyl (MMT), is used as an octane-enhancing agent in unleaded petrol in Canada, the United States of America (USA), Europe, Asia, and South America [3]. Some manganese compounds are used in fertilizers, varnish, and fungicides and as livestock feeding supplements. All these activities lead to anthropogenic causes for Mn contamination of water sources. Manganese is found in abundance on earth's crust and usually present in the form of compounds, rather than the elemental form. In the compounds, "Mn" is present in different oxidation states such as Mn^{2+}, Mn^{4+}, or Mn^{7+} (USEPA, 1994) [4]. It is generally present in groundwater as Mn^{2+} and is considered a pollutant beyond a certain limit, because of its organoleptic properties. According to the World Health Organization, the maximum acceptable "Mn" concentration in drinking water is 0.05 mg/l [WHO, 2011] [5, 6]. According

to Indian Standard (IS), 10500 :2012, the acceptable limit for Mn in drinking water is 0.1 mg/l.

In surface waters, manganese occurs in both dissolved and suspended forms, while in groundwater, it remains in a dissolved state [7]. Mn is mainly formed by hydrogeochemical reactions and is found in the form of hydroxides, sulfates, or carbonates of the divalent Mn^{2+} ion. Thus, anaerobic groundwater often contains elevated levels of dissolved manganese. The divalent form (Mn^{2+}) predominates in most water at pH 4–7, but at higher pH values, more highly oxidized forms may occur [8]. Upon exposure to air, Mn^{2+} forms MnO_2 particulates that can cause black or brown stains on household utensils, plumbing fixtures, and clothing. Mn otherwise is an essential nutrient, and research findings indicated that [9] a minimum quantity of 3.5–7 mg/day for adults is necessary for regular physiological functions [9]. But, a higher concentration of Mn^{2+} in drinking water is hazardous for health which may cause damage to the central nervous system and neurological systems in humans [10]. This may even result in Parkinson's disease [11, 12]. Excess manganese ion concentration in drinking water imparts an unpleasant metallic taste, stains plumbing fixtures, and also leads to discoloration of water and laundry [13]. Similarly, when manganese(II) in solution undergoes oxidation, it gets precipitated, resulting in encrustation problems and may damage the water storage tanks and pipelines by forming coating [14, 15].

Thus, several physical, chemical, and biological Mn remediation strategies have been developed over the last few decades to mitigate the toxic effects of excess Mn and to ensure a safe supply of drinking water.. Currently, many treatment methods, such as oxidation [16–19], membrane filtration [20], and adsorption [21–24], are employed in removing high manganese concentrations from groundwater [25]. Although the oxidation method can remove manganese rapidly, the generation of some toxins demonstrates the disadvantages of this method.

Membrane filtration [26–29] is an effective method for heavy metal removal, but it has the limitations like a requirement of specific pH, which accelerates membrane fouling [15, 16]. An adsorption technique however has appeared to be more economical and has received extensive attention for the removal of manganese from groundwater [30, 31]. The application of the adsorption method is highly dependent on the adsorptive materials [32]. Some natural materials like zeolites, chitosan, and clay are known as low-cost materials that are used for the purpose [33]. Especially, zeolites, the low-cost materials with exceptional ion exchange and sorption properties, can abundantly be used [34, 35]. However, pH has a significant impact on the ion exchange properties of these highly porous zeolite-based materials, which may even sometimes negate its cost economic nature.

Therefore, the development of new highly porous and highly efficient cost economic materials for removal of cations from drinking water sources is important to research objectives and many scientific interests are focused on that. Manganese oxide has been successfully used as a catalytic adsorbent for the removal of manganese [36]. But this too has certain strict limitations that restrict its use as an adsorbent for manganese removal. Immobilization of manganese oxide on materials like sand [25], clay [37], zeolites [38–40], active carbon [41, 42], and glass beads [43] has been carried out, and these MnO-coated materials are used as a catalyst for effective removal of Mn from water. The MnO-coated sand showed the best results in the pH range of 5.5 to 8.0. Mn^{2+} uptake also increased with increasing temperature from 25 to 45°C. The study also showed that the mechanism was chemisorption. The equilibrium adsorption data were best represented by the Langmuir isotherm [25]. Similarly, MnO-coated zeolite (MOCZ) materials are also known which have a good binding affinity and hence strong adsorption capacity for Mn^{2+} ions [40]. Other known MnO-coated zeolite showed maximum removal of Mn at pH 7, with an Mn concentration of 5 mg/l. The equilibrium adsorption data were best represented by the Langmuir isotherm, indicating monolayer adsorption on a homogenous surface, and the adsorption capacity was found to be 0.21 mg/g at 20°C. It was assumed that the adsorption process was controlled by physical mechanism rather than chemical [39]. Zohreh and Abedi investigated the efficiency of impregnated active carbon in manganese removal from aqueous solutions which showed highest adsorption of Mn^{2+} ions at the pH of 9 (Mn^{2+} removal: 67.19%) with the adsorption kinetics fitting the pseudo-second-order and intraparticle diffusion models. They confirmed the suitability of the Langmuir model for Mn^{2+} adsorption using impregnated active carbon [42]. The manganese is also being removed by using MnO-coated glass beads, which are developed using dry and wet coating techniques [43]. In most of the cases, pH has a decisive role in the Mn^{2+} removal process.

In the present study, we have attempted to utilize manganese oxide-coated hollow polymethylmethacrylate microspheres, to develop a low-cost and highly efficient novel adsorbent (MHPM) for the removal of Mn contaminant from water. The adsorption capacity of MHPM was evaluated by adsorption isotherm studies as a function of parameters such as pH, initial ion concentration, and contact time. Langmuir and Freundlich isotherm parameters were determined and compared. Therefore, the main objectives of this work were to investigate the ability of manganese removal onto MHPM and to reveal a probable removal mechanism of manganese from the contaminated water.

2. Materials and Methods

2.1. Materials. Polymethylmethacrylate (PMMA) [Sigma-Aldrich, MW (avr.): 120,000, 98%, viscosity 0.20 g/dl (lit.)], dichloromethane [Merck, mfg date: Jan 2013, 99.5%, M = 84.93 g/mol], polyvinyl alcohol [Central Drug House, Delhi, MW (avr.): 125,000, 99.25% viscosity 35-50 cP at 4% cold aqueous solution], acetic acid [Merck, M = 60.052 g/mol], manganese(II) sulfate ($MnSO_4$) [Aldrich, M = 151.001 g/mol], and potassium permanganate ($KMnO_4$) solution [Aldrich, M = 158.034 g/mol] were used. All other reagents used are of analytical grade and were obtained from Aldrich, India. The limestone was acquired from the mining site, Meghalaya, India.

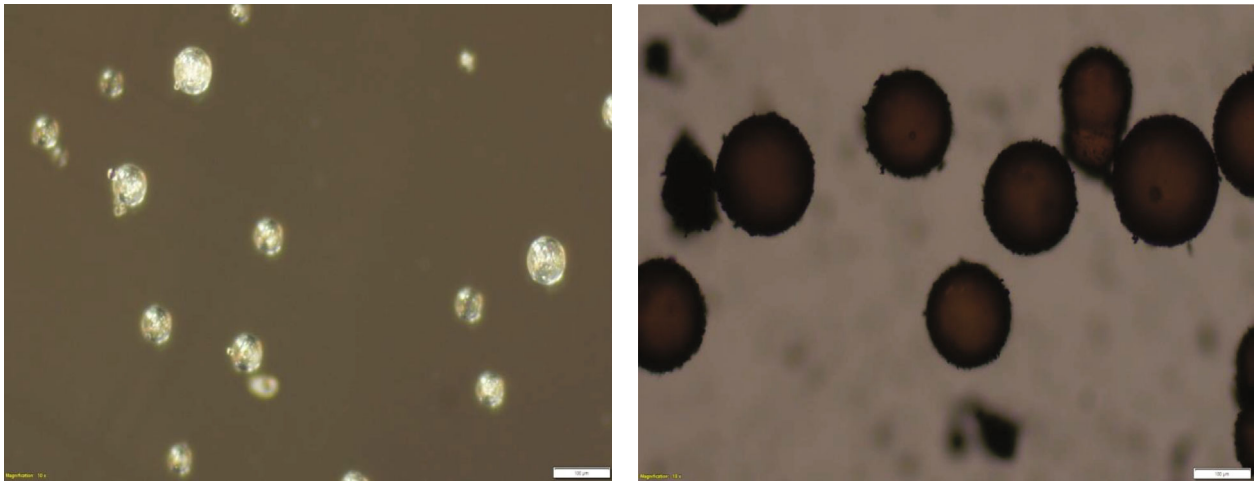

(a) (b)

Figure 1: Optical micrographs of (a) uncoated and (b) MnO-coated hollow PMMA MS.

2.2. Preparation of HPM Microspheres. The solvent evaporation technique [44] is used to synthesize hollow PMMA microspheres. In the first step, a solution was prepared by dissolving PMMA (5-6% *w*/*v*) in dichloromethane with the help of a magnetic stirrer. The solution was then added dropwise to a stirring aqueous medium. The aqueous medium comprises (0.5%, *w*/*v*) of poly(vinyl alcohol) which acts as a stabilizer. The stirring is maintained at 550 rpm with a propeller-type mechanical stirrer. PMMA microspheres (HPM) are formed by slow evaporation of dichloromethane at room temperature. At the end of the reaction, hollow PMMA microspheres are obtained after washing with water and drying at 70°C. The bulk density of the HPM is calculated as 0.69 gm/cc.

2.3. Preparation of MHPM. The manganese oxide-coated PMMA was synthesized, in a 1 l beaker. In the primary step, a solution is prepared by adding 10 g of PMMA to 250 ml of 2 N acetic acid containing 0.5 M $MnSO_4$. The solution was stirred as 200 ml of 0.43 M potassium permanganate solution was added. The coated material was settled before air drying at 30°C, was rinsed with Milli-Q water, and was redried. The obtained yield is 72%. Then, the product was stored in an amber glass bottle.

2.4. Characterization of Materials. The synthesized materials were characterized by a scanning electron microscope with energy-dispersive X-ray analysis attachment (Carl Zeiss, EVO50), a FTIR (Bruker model Alpha-T), an optical microscope with Leica DMLM/P (Leica Microsystems AG Switzerland at 50x magnification), an transmission electron microscope (TEM) (JEOL 200 kV model no. JEE2100), and thermogravimetric analysis (TGA) (TA Instruments, USA; model 2950 and 2910). FTIR of the samples was taken with the help FTIR spectrophotometer (Bruker Alpha model with KBr). X-ray diffraction patterns were measured with XRD (model: Rigaku Ultima IV IR Technology Services Pvt. Ltd., in powder mode with Cu and Mo with Kβ filter). The UV-visible spectrophotometer is a double beam spectrophotometer from Analytik Jena Model SPECORD 205 (via standard IS 3025 (Part 59): 2006).

3. Results and Discussion

3.1. Characterization of HPM and MHPM

3.1.1. Optical Microscope Analysis. The optical micrographs in Figure 1 show the micrographs for uncoated PMMA (HPM) and MnO-coated microspheres (MHPM). The micrograph of uncoated hollow polymethylmethacrylate microspheres is of white-colored spheres with different sizes. On the contrary, with clear distinction, the MnO-coated microspheres are appeared in pinkish-brown/dark brown color due to the deposition of MnO on the surface of HPM microspheres. Thus, the color difference between the coated (MHPM) and uncoated (HPM) microspheres confirms the presence of MnO coating on the surface of microspheres.

3.1.2. SEM Analysis. The SEM images in Figure 2 are captured by a scanning electron microscope with X-ray diffraction analysis attachment. These SEM micrographs are used to analyze the surface morphology of MHPM. The SEM micrographs illustrate that the diameter of the HPM microspheres is in the range of 20–80 μm. The micrographs of uncoated HPM microspheres show the smooth surface of microspheres, whereas the surface of MnO-coated HPM microspheres shows the occurrence of a precipitate of MnO, i.e., manganese oxide formed as clusters on to the polymer surface, leading to surface roughness of microsphere. Hence, SEM micrographs indicate the presence of MnO coating on HPM surface.

3.1.3. TEM Analysis. Figure 3 shows the TEM images of HPM and MHPM. The image textures for the HPM and MHPM are completely different. The image for HPM shows a smooth kind of feature, whereas the image for MHPM shows well-dispersed MnO particles throughout the polymeric matrix. Hence, in general, a good dispersion of MnO particles was obtained except for particle aggregation at some places which

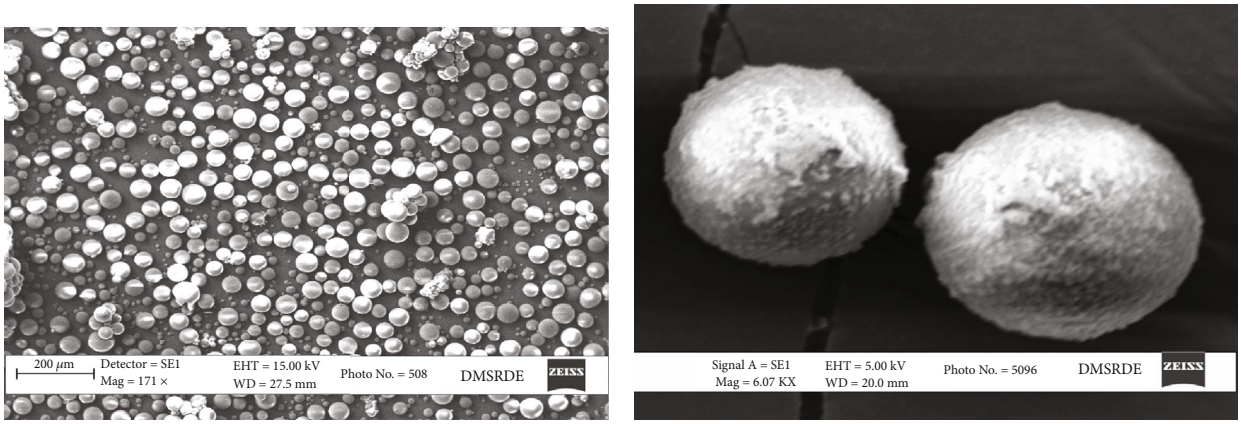

(a) (b)

Figure 2: SEM micrographs of (a) uncoated and (b) MnO-coated hollow PMMA MS.

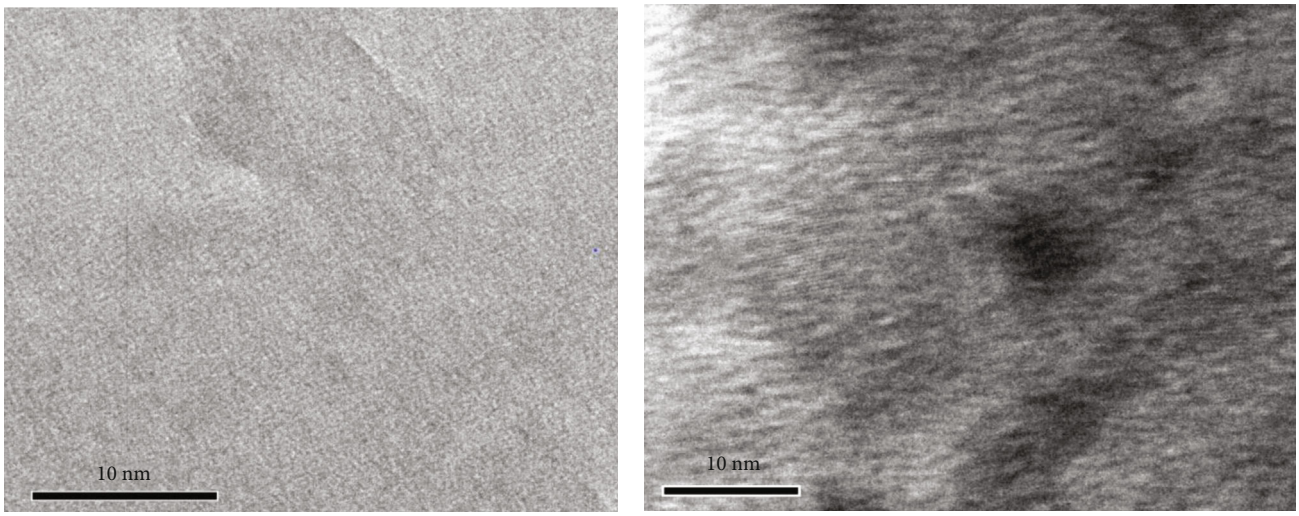

(a) (b)

Figure 3: TEM micrographs of (a) uncoated and (b) MnO-coated hollow PMMA MS.

is difficult to avoid for small particles. Aggregation of the MnO particles also influences the aspect ratio (average diameter may change) which in turn may influence the surface texture of the polymeric microspheres. There are possibilities of overlapping of MnO particles along the depth direction of the specimen (i.e., Z-direction) resulting in observation of poor resolution along this direction for the TEM images. The study confirms a random coating of the MnO on the surface of PMMA. The uneven surface confirms physical interaction rather than chemicals between the particles and polymeric surfaces. This has further been confirmed by the isotherm studies.

3.1.4. XRD Analysis. The XRD diffraction patterns of HPM and MHPM are displayed in Figure 4. A broad and shallow peak at around 2θ of 16° is a typical feature of amorphous PMMA. The diffraction curve of MHPM shows peaks at around 2θ of 12°, 24°, 37°, and 66°. Besides, the weak diffraction intensity of the samples reveals a poor crystallization or amorphous form of the MnO_2-based materials prepared by a facile chemical technique.

The patterns of native and impregnated active carbon implied the formation of manganese oxide. The Mn-coated PMMA is confirmed by the peaks at 2θ of 23° and 36° (Figure 4). According to the ICDD 00-012-0720 data, the peaks appeared at 2θ of 23° and 36°, indicating the presence of manganese oxide [45].

3.1.5. TGA Analysis. TGA curves of HPM and MHPM are displayed in Figure 5. The curve shows that there is a slight weight loss during initial heating up to 85°C for both the materials which can be assigned to traces of moisture present in the sample. The decomposition temperature of PMMA is observed to be in the range of 230°C to 420°C, and complete decomposition was observed at 420°C. A similar trend of weight loss was displayed by MnO-coated HPM except for the residual weight of 8.9%. This residual weight corresponds to MnO coating. Thermal analysis of the materials thus confirms good hydrothermal stability of the materials.

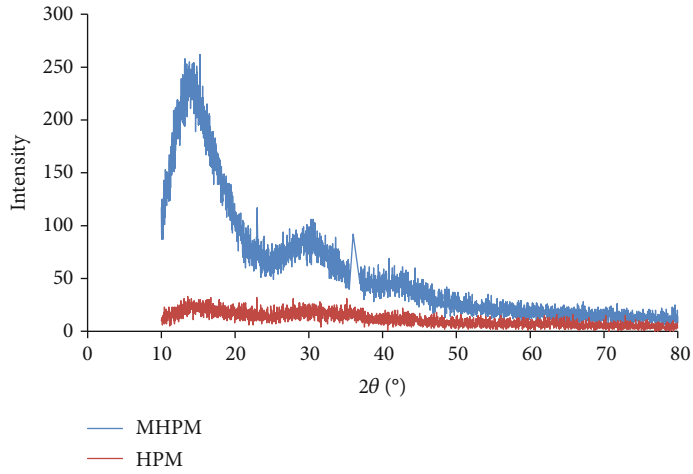

Figure 4: X-ray diffraction (XRD) patterns of HPM (red) and MHPM (blue).

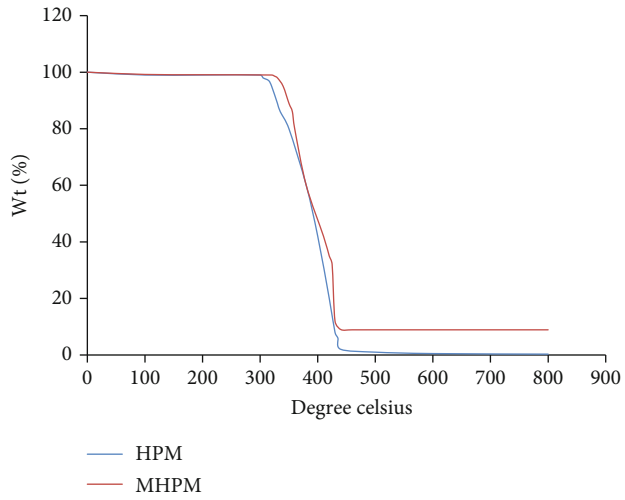

Figure 5: TGA analysis of HPM (blue) and MHPM (red).

3.1.6. FTIR Analysis. The presence of MnO on the HPM microsphere can also be analyzed using FTIR spectroscopy. The FTIR spectra of HPM and MHPM are shown in Figure 6. The sharp bands observed at wavelengths lower than 750 cm^{-1} are attributed to Mn–O stretching of MnO [16]. The two bands that appeared at 515 and 480 cm^{-1} of the FTIR spectra can be associated with the Mn-O bond and thus confirming the deposition of Mn over the polymeric surface of PMMA. After adsorption, MHPM exhibited an extra band at 515 cm^{-1}, which corresponds to the Mn-O bond.

3.2. Optimization of Adsorption Parameters

3.2.1. Effect of Contact Time. A time-dependent study of Mn removal was carried out as shown in Figure 7. The removal shows a gradual increase with increasing time, and complete effectiveness was obtained within 70 min. After 70 min, it gets almost saturated. The experiment is carried out for the maximum initial concentration of Mn of 150 mg/l as compared to other adsorption tests. This is in accordance with previously reported literature [46].

3.2.2. Effect of Mn Concentration on % Removal and Adsorption Capacity. An experiment was carried out on MnO-coated hollow polymethylmethacrylate microspheres (MHPM) to investigate the effects of Mn concentration on the percentage removal of Mn^{2+} from the aqueous solution. The initial concentration of Mn was chosen as 20 mg/l, 30 mg/l, 50 mg/l, 100 mg/l, and 150 mg/l, respectively, at five different contact times. The percentage removal of Mn^{2+} from aqueous solution at equilibrium time was noted as 98.7%, 86.04%, 82.05%, 77.31%, and 55.14%, respectively, for the above solutions. This shows with an increase in initial concentration, the adsorption capacity of MHPM decreases.

This fact is represented in Figure 8(a), which shows that with an increase in initial concentration of Mn(II) ions in solution, percentage removal of Mn^{2+} from aqueous solution decreases. The decrease in removal efficiency is due to the unavailability of active sites on MHPM for the adsorption of the metal ions onto it. The variations of these concentrations are small at the low concentrations and increase more significantly with the increase in concentration. This is occurring because the ratio of available metal ions to the available active sites is small at low initial concentrations.

The adsorption capacity for 20 mg/l initial concentration of Mn(II) in aqueous solution was evaluated as 1.974 mg/g from Figure 8(b). The same was found to increase to 2.7012 mg/g for 30 mg/l of Mn(II) ion concentration in aqueous solution and was continuously increasing until an equilibrium adsorption capacity for Mn(II) ion was reached at around 8.3 mg/g. From this data, it is inferred that adsorption capacity varies with the initial concentration of the Mn(II) in an aqueous solution. This is due to the available binding site on the surface of the PMMA microsphere in the initial stage where the binding site is in a higher amount than the Mn(II) in solution. But once the binding sites are saturated at a higher concentration of the Mn(II) in solution, the absorption capacity also reached its saturation. This is an indication of the monolayer adsorption mechanism.

3.2.3. Effect of pH on Adsorption Capacity. As it can be observed in Figure 9, Mn^{2+} adsorption by the MHPM is less

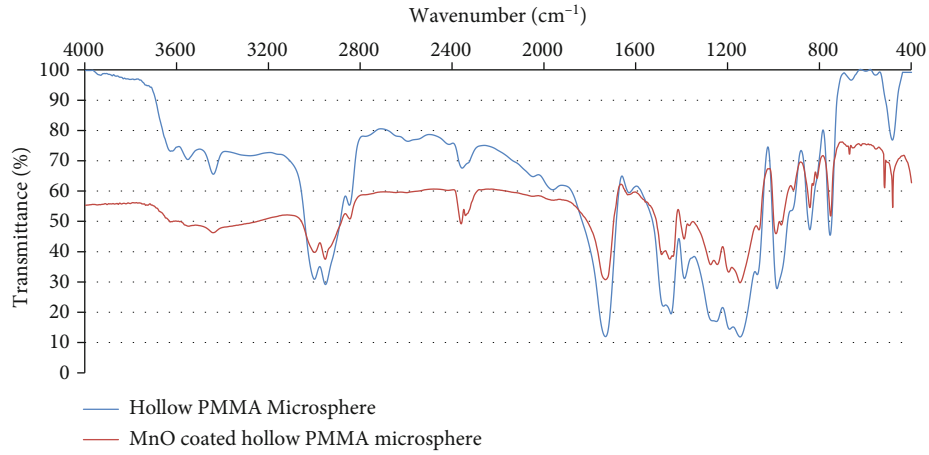

Figure 6: FTIR analysis of HPM and MHPM.

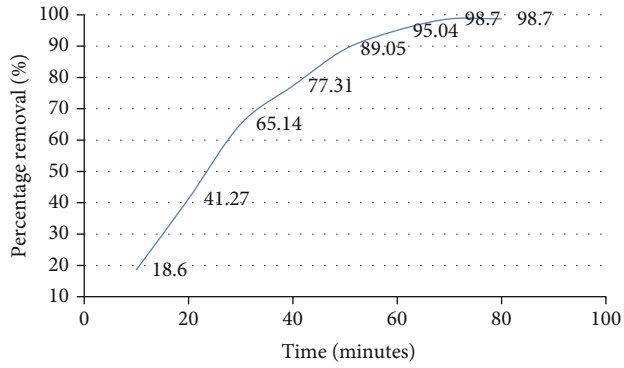

Figure 7: Effect of contact time of Mn(II) on % removal.

significant in the lower pH range. This happens possibly due to the fact that at lower pH, there is a competition between the H^+ ion and Mn^{2+} ions for the available exchangeable sites on MHPM and due to the preponderance of H^+ ions, it wins the race. With an increase in pH, there is a concomitant increase in negative charge density on the MHPM surface causing deprotonation of the metal-binding sites, and eventually, Mn^{2+} ion adsorption increases. Beyond pH 8.0, we can observe a dramatic increase in the uptake capacity of Mn^{2+} ions by MHPM and this is continued up to pH 9.0. Beyond this value, Mn^{2+} ions predominantly remain in the precipitate form, and therefore, uptake of Mn^{2+}ions by MHPM is impossible.

The dynamic increment in Mn expulsion as the suspension turns out to be progressively basic can be clarified by an expansion in the number of adsorption destinations. In the fluid arrangement, MnO present a hydroxylated surface whose charge is firmly pH reliant. As pH increases, surface negative charge increases due to the deprotonation of functional surface reunions (OH^-) and electrostatic forces bring cations into the surface. Actually, at low pH, prevailing H^+ particle arrangements possess the restricting destinations of adsorbent, bringing about a net positive surface charge that forestalls cation adsorption.

3.3. Adsorption Isotherms. An adsorption isotherm represents the plot between the amount of solute adsorbed onto the solid and the equilibrium concentration of the solute in solution at a given temperature [47]. The adsorption isotherms indicate the distribution of adsorbate and adsorbent at equilibrium conditions for the adsorption process. These isotherms are represented in the form of graphical plots which set up a relationship between the equilibrium concentration of a solute on the surface of an adsorbent (q_e) to the concentration of the solute in the liquid (C_e), with which it is in contact. The nature of the adsorption process can be obtained from these plots. Langmuir and Freundlich adsorption isotherm models are used here to describe the metal ion distribution between the solid and liquid phases. The efficiency of synthesized MHPM to remove Mn(II) from water is determined by using these isotherm adsorption models.

3.3.1. Langmuir Isotherm. The Langmuir isotherm is suggested when all the adsorption active sites are occupied and further adsorption process is terminated. Therefore, this isotherm is used to establish equilibrium between adsorbate and adsorbent in the given system, where the partial pressure of the adsorbate approaches saturation [48]. At this saturation point, all the active sites are equally energetic and there is no interaction among the adsorbed molecules and the neighboring sites [49].

From Figure 6(b), it has been observed that for MHPM material, the equilibrium point was found at 150 mg/l and corresponds to 8.27 mg/g. From this result, it is assumed that the Langmuir model is best fitted at a higher concentration of adsorbate. At equilibrium conditions, the linear form of the Langmuir equation is given as follows:

$$\frac{q_e}{C_e} = K_L q_m - K_L q_e, \quad (1)$$

where q_e (mg/g) is the amount of Mn(II) adsorbed, C_e (mg/l) is the concentration of the Mn(II) solution, K_L is the Langmuir constant related to adsorption enthalpy, and q_m is the maximum adsorption capacity.

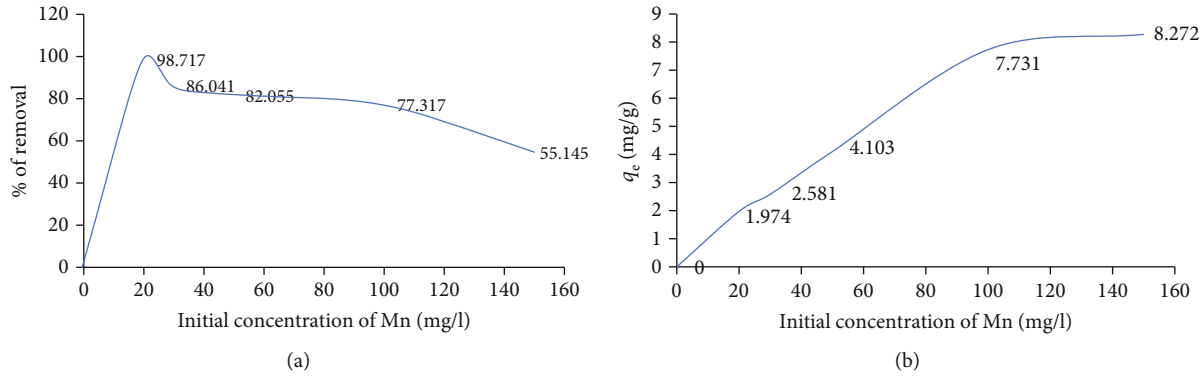

Figure 8: Effect of the initial concentration of Mn(II) on (a) % removal and (b) adsorption capacity.

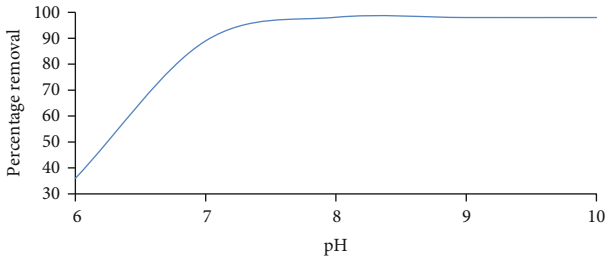

Figure 9: Effect of pH on % removal of Mn(II).

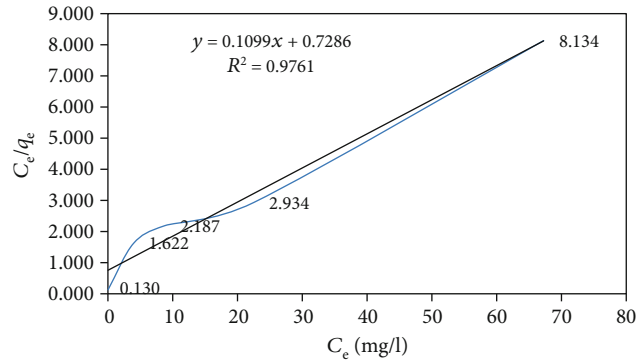

Figure 10: Langmuir adsorption isotherm.

From Figure 10, it is shown that the Langmuir model is an empirical model having a linear plot, which indicates that the active sites on the surface are inadequate and the monolayer of MHPM is fitted into the heterogeneous surface. The capability of removing a certain amount of manganese ions by using synthesized MnO-coated HPM is described as the adsorption capacity (q_e) of the particular adsorbent. The adsorption capacity is mathematically represented as follows:

$$q_e = X/M \tag{2}$$

where X is the amount of adsorbate (Mn in water) and M is the weight of adsorbent (manganese-coated PMMA).

The capacity to retain the maximum amount of manganese (adsorbate) per unit mass of MHPM (adsorbent) is described as maximum adsorption capacity (q_m). Usually, the q_m is achieved at low concentrations and rarely achieved at high concentrations. The enthalpy of the adsorption is correlated with the Langmuir isotherm constant (K_L in g/l) which describes the affinity of MHPM towards Mn(II) ions. From Equation (1), we obtain intercept as q_m and slope as K_L. The favorable conditions of adsorption are indicated by correlation coefficient R^2, whose value should be equal to 1. From the experimental results on MHPM, the obtained maximum adsorption capacity (q_m) is 8.374 mg/g, the value of Langmuir constant (K_L) is 1.201 mg/l, and R^2 value is obtained as 0.976. The Langmuir isotherm parameters obtained from adsorption data are listed in Table 1.

The characteristics of Langmuir isotherm are evaluated by a value of a separation factor R_L. This separation factor R_L is inversely proportional to adsorption capacity (q_e). As the adsorption capacity increases, the corresponding separation factor decreases thereby confirms that the isotherm model is well fitted and adsorption is favorable.

$$q_e = 1/[1 + (R_L + C_o) \tag{3}$$

In Figure 11, a graph is plotted between separation factor R_L and adsorption capacity (q_e) which shows that separation factor depends upon the initial concentration of adsorbents in the solution. The figure represents that the separation factor decreases with the increase of initial concentration from 0.039 at 20 mg/l to 0.026 at 30 mg/l. In this case, the adsorption is said to be favorable as the R_L value is less than 1 [47, 50, 51]. Therefore, this model is well fitted to the obtained adsorption data.

3.3.2. Freundlich Isotherm. The Freundlich isotherm model suggests the multilayer adsorption and describes the adsorption on a heterogeneous surface [35, 52]. During the adsorption process, all the active sites on the adsorbent are filled with adsorbate, and therefore, the energy of adsorption declines exponentially. The obtained plot of the Freundlich isotherm is shown in Figure 9. Mathematically, the isotherm is represented as follows:

$$\log q_e = \log K_F + (1/n) \log C_e \tag{4}$$

Table 1: Langmuir isotherm parameters.

Langmuir isotherm	q_m (mg/g)	K_L (mg/l)	R^2
	8.374	1.201	0.976

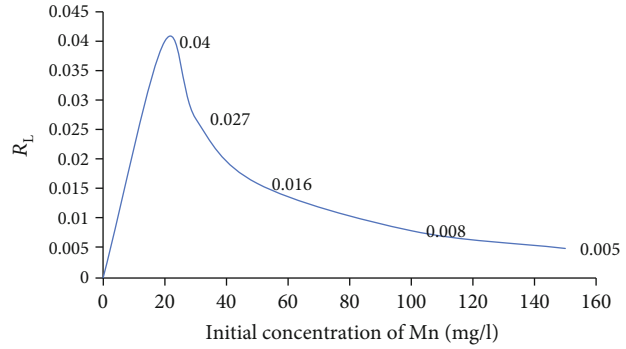

Figure 11: Langmuir isotherm for adsorption of Mn(II) ion on MnO-coated HPM surface.

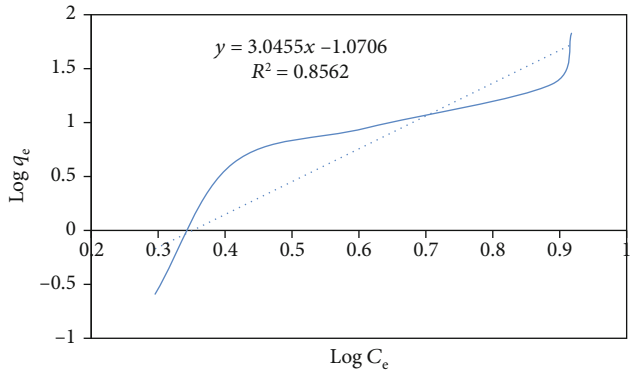

Figure 12: Freundlich isotherm as a plot of log q_e versus log C_e.

where the adsorption capacity and the adsorption intensity are given as "K_F" and "n", respectively, which are also known as Freundlich constants.

$1/n$ is given as heterogeneity factor and "n" is a measure of the deviation from the linearity of adsorption.

The slope and the intercept obtained from the graph (Figure 12) plotted between log q_e and log C_e give adsorption intensity ($1/n$) and adsorption capacity (K_F), respectively. The values of $1/n$ also indicate the favorability and capacity of the adsorbate/adsorbent system.

From the experiments conducted on MHPM, the obtained value of "n" is 3.897. Generally, the value of n should be greater than 1 in case of higher surface density as the surface sites of the adsorbent are distributed inadequately to the adsorbate (manganese ions). As a result, the adsorption process is favorable when $n > 1$. The affinity of adsorbent (MHPM) towards the adsorbate (manganese) is denoted by the value of K_F. At higher values of K_F, there is a strong binding between adsorbate molecules and the surface adsorbent. In this case, the R^2 value obtained for MHPM was 0.856 which is low compared to the Freundlich correlation factor, where R^2 is 1.

Table 2: Freundlich isotherm parameters.

Freundlich isotherm	$1/n$	n	K_F (mg/l)	R^2
	0.257	3.897	2.801	0.856

As shown in Table 2, Freundlich isotherm is an empirical model that fits the logarithm data well in the equation, but the obtained R^2 value as 0.856 is very low and thus proved that adsorption data is best fitted in the case of Langmuir isotherm. This is due to the separation factor of R_L which establishes the high efficiency of Langmuir isotherm. Previous studies reported in the literature [34, 35, 40] on other adsorbents (e.g., zeolites) exhibited a good fit of the experimental data to the Langmuir isotherm, suggesting the existence of a plateau region where no further increase in Mn adsorption exists.

4. Conclusion

We have successfully immobilized manganese oxide on HPM, to exploit its adsorption efficiency for the removal of Mn^{2+} ions from an aqueous solution. Although manganese oxide directly can be used as an adsorbent for removal of Mn^{2+} from an aqueous solution, it causes lots of inconveniences because it exists in the powder form in water. We have succeeded in overcoming this limitation. The material developed will have significant industrial utility since MHPM apart from being very economical is a lightweight material and offers high surface area compared to other materials used for the purpose. The manganese removal is influenced by various operational parameters such as pH, contact time, and initial concentrations. The most notable feature of the material is that for manganese concentrations from 20 to 50 mg/l, the removal efficiency was >82%. Further at higher pH, the material exhibits remarkable separation efficiency for Mn^{2+} ions from an aqueous solution. Even at a higher concentration of Mn^{2+} ions, the material shows maximum adsorption capacity, a quality rarely observed with other materials of this kind. Adsorption isotherm studies reveal that the adsorption efficiency of Mn(II) metal ions on MHPM is described by Langmuir and Freundlich isotherm models, and Langmuir isotherm provides the best fit. From the above results, we can conclude that this novel adsorbent MnO-coated HPM removes Mn ions from water resources efficiently.

Data Availability

All data is available in the manuscript.

Conflicts of Interest

The authors declare no competing financial or personal interests.

Acknowledgments

The authors would like to acknowledge the kind help of the director of DRL and the director and testing team of DMSRDE, Kanpur, along with the director and faculty members of NIT Nagaland for the guidance and help in this research work.

References

[1] M. Williams-Johnson, *World Health Organization Geneva*, World Health Organization (WHO), 1999.

[2] M. Bethesda, "HSDB (2001) Manganese compounds," 2001, http://toxnet.nlm.nih.gov/cgi-bin/sis/htmlgen?HSDB.

[3] D. R. Lynam, J. W. Roos, G. D. Pfeifer, B. F. Fort, and T. G. Pullin, "Environmental effects and exposures to manganese from use of methylcyclopentadienyl manganese tricarbonyl (MMT) in gasoline," *Neurotoxicology*, vol. 20, no. 2–3, pp. 145–150, 1999.

[4] A. M. Dietrich and G. A. Burlingame, "Critical review and rethinking of USEPA secondary standards for maintaining organoleptic quality of drinking water," *Environmental Science & Technology*, vol. 49, no. 2, pp. 708–720, 2015.

[5] C. K. Tay and E. Hayford, "Levels, source determination and health implications of trace metals in groundwater within the Lower Pra Basin, Ghana," *Environmental Earth Sciences*, vol. 75, no. 18, 2016.

[6] World Health Organization, "Guidelines for Drinking-Water Quality, Fourth Edition," 2011, 2020, https://www.who.int.

[7] N. Esfandiar, B. Nasernejad, and T. Ebadi, "Removal of Mn(II) from groundwater by sugarcane bagasse and activated carbon (a comparative study): application of response surface methodology (RSM)," *Journal of Industrial and Engineering Chemistry*, vol. 20, no. 5, pp. 3726–3736, 2014.

[8] 2000 A, "Toxicological profile for manganese," in *ATSDR's Toxicological Profiles*, Agency for Toxic Substances and Disease Registry, U.S. Department of Health and Human Services (Public Health Service), 2002.

[9] J. H. Freeland-Graves and C. W. B. F. Bales, "Manganese requirements of humans," *Nutritional bioavailability of manganese*, C. Kies, Ed., pp. 90–104, ACS Publications, 1987.

[10] M. Han, Z.-W. Zhao, W. Gao, and F.-Y. Cui, "Study on the factors affecting simultaneous removal of ammonia and manganese by pilot-scale biological aerated filter (BAF) for drinking water pre- treatment," *Bioresource Technology*, vol. 145, pp. 17–24, 2013.

[11] R. J. F. Elsner and J. G. Spangler, "Neurotoxicity of inhaled manganese: public health danger in the shower?," *Medical Hypotheses*, vol. 65, no. 3, pp. 607–616, 2005.

[12] H. A. Roels, R. M. Bowler, Y. Kim et al., "Manganese exposure and cognitive deficits: a growing concern for manganese neurotoxicity," *NeuroToxicology*, vol. 33, no. 4, pp. 872–880, 2012.

[13] A. E. Griffin, "Significance and removal of manganese in water supplies," *Journal - American Water Works Association*, vol. 52, no. 10, pp. 1326–1334, 1960.

[14] E. L. Bean, "Potable water-quality goals," *Journal - American Water Works Association*, vol. 66, no. 4, pp. 221–230, 1974.

[15] M. Sri Abirami Saraswathi, K. Divya, P. Selvapandian, D. Mohan, D. Rana, and A. Nagendran, "Permeation and antifouling performance of poly (ether imide) composite ultrafiltration membranes customized with manganese dioxide nanospheres," *Materials Chemistry and Physics*, vol. 231, pp. 159–167, 2019.

[16] A. Funes, J. de Vicente, L. Cruz-Pizarro, and I. de Vicente, "The influence of pH on manganese removal by magnetic microparticles in solution," *Water Research*, vol. 53, pp. 110–122, 2014.

[17] A. G. Tekerlekopoulou, I. A. Vasiliadou, and D. V. Vayenas, "Biological manganese removal from potable water using trickling filters," *Biochemical Engineering Journal*, vol. 38, no. 3, pp. 292–301, 2008.

[18] S. Wagloehner, M. Nitzer-Noski, and S. Kureti, "Oxidation of soot on manganese oxide catalysts," *Chemical Engineering Journal*, vol. 259, pp. 492–504, 2015.

[19] L. Yang, X. Li, Z. Chu, Y. Ren, and J. Zhang, "Distribution and genetic diversity of the microorganisms in the biofilter for the simultaneous removal of arsenic, iron and manganese from simulated groundwater," *Bioresource Technology*, vol. 156, pp. 384–388, 2014.

[20] H. Jia, J. Liu, S. Zhong et al., "Manganese oxide coated river sand for Mn(II) removal from groundwater," *Journal of Chemical Technology & Biotechnology*, vol. 90, no. 9, pp. 1727–1734, 2015.

[21] M. Abdel Salam, "Synthesis and characterization of novel manganese oxide nanocorals and their application for the removal of methylene blue from aqueous solution," *Chemical Engineering Journal*, vol. 270, pp. 50–57, 2015.

[22] M. E. Goher, A. M. Hassan, I. A. Abdel-Moniem, A. H. Fahmy, M. H. Abdo, and S. M. El-Sayed, "Removal of aluminum, iron and manganese ions from industrial wastes using granular activated carbon and Amberlite IR-120H," *Egyptian Journal of Aquatic Research*, vol. 41, no. 2, pp. 155–164, 2015.

[23] S.-L. Lo, H.-T. Jeng, and C.-H. Lai, "Characteristics and adsorption properties of iron-coated sand," *Water Science and Technology*, vol. 35, no. 7, pp. 63–70, 1997.

[24] C. Luo, Z. Tian, B. Yang, L. Zhang, and S. Yan, "Manganese dioxide/iron oxide/acid oxidized multi-walled carbon nanotube magnetic nanocomposite for enhanced hexavalent chromium removal," *Chemical Engineering Journal*, vol. 234, pp. 256–265, 2013.

[25] C. C. Kan, M. C. Aganon, C. M. Futalan, and M. L. P. Dalida, "Adsorption of Mn2+ from aqueous solution using Fe and Mn oxide-coated sand," *Journal of Environmental Sciences (China)*, vol. 25, no. 7, pp. 1483–1491, 2013.

[26] F. Khan, R. Wahab, M. Rashid et al., "The use of carbonaceous nanomembrane filter for organic waste removal," in *Application of Nanotechnology in Water Research*, pp. 115–152, Wiley Blackwell, 2014.

[27] A. K. Mishra, *Application of Nanotechnology in Water Research*, A. K. Mishraed, Ed., John Wiley & Sons, Inc., Hoboken, NJ, USA, 2014.

[28] J. E. Tobiason, A. Bazilio, J. Goodwill, X. Mai, and C. Nguyen, "Manganese removal from drinking water sources," *Current Pollution Reports*, vol. 2, no. 3, pp. 168–177, 2016.

[29] K. Zodrow, L. Brunet, S. Mahendra et al., "Polysulfone ultrafiltration membranes impregnated with silver nanoparticles show improved biofouling resistance and virus removal," *Water Research*, vol. 43, no. 3, pp. 715–723, 2009.

[30] A. Ates, "Role of modification of natural zeolite in removal of manganese from aqueous solutions," *Powder Technology*, vol. 264, pp. 86–95, 2014.

[31] R. Han, Z. Lu, W. Zou, W. Daotong, J. Shi, and Y. Jiujun, "Removal of copper(II) and lead(II) from aqueous solution by manganese oxide coated sand: II. Equilibrium study and competitive adsorption," *Journal of Hazardous Materials*, vol. 137, no. 1, pp. 480–488, 2006.

[32] S. Zhang, Y. Lu, X. Lin, X. Su, and Y. Zhang, "Removal of fluoride from groundwater by adsorption onto La(III)- Al(III) loaded scoria adsorbent," *Applied Surface Science*, vol. 303, pp. 1–5, 2014.

[33] S. Babel and T. A. Kurniawan, "Low-cost adsorbents for heavy metals uptake from contaminated water: a review," *Journal of Hazardous Materials*, vol. 97, no. 1-3, pp. 219–243, 2003.

[34] M. K. Doula, "Removal of Mn2+ ions from drinking water by using clinoptilolite and a clinoptilolite-Fe oxide system," *Water Research*, vol. 40, no. 17, pp. 3167–3176, 2006.

[35] E. Erdem, N. Karapinar, and R. Donat, "The removal of heavy metal cations by natural zeolites," *Journal of Colloid and Interface Science*, vol. 280, no. 2, pp. 309–314, 2004.

[36] J. C. Xu, G. Chen, X. F. Huang et al., "Iron and manganese removal by using manganese ore constructed wetlands in the reclamation of steel wastewater," *Journal of Hazardous Materials*, vol. 169, no. 1–3, pp. 309–317, 2009.

[37] J. A. Alexander, M. A. A. Zaini, S. Abdulsalam, U. Aliyu El-Nafaty, and U. O. Aroke, "Isotherm studies of lead(II), manganese(II), and cadmium(II) adsorption by Nigerian bentonite clay in single and multimetal solutions," *Particulate Science and Technology*, vol. 37, no. 4, pp. 403–413, 2019.

[38] J. Jeż-Walkowiak, Z. Dymaczewski, A. Szuster-Janiaczyk, A. Nowicka, and M. Szybowicz, "Efficiency of Mn removal of different filtration materials for groundwater treatment linking chemical and physical properties," *Water (Switzerland)*, vol. 9, no. 7, p. 498, 2017.

[39] M. Mohamadreza and K. Maryam, "Absorption isotherm study of Mn2+ on MnO2 and FeO - coated zeolite from aqueous solution," *International Journal of Advanced Science and Technology*, vol. 72, pp. 63–72, 2014.

[40] S. R. Taffarel and J. Rubio, "Removal of Mn2+ from aqueous solution by manganese oxide coated zeolite," *Minerals Engineering*, vol. 23, no. 14, pp. 1131–1138, 2010.

[41] A. Itodo, H. Itodo, and M. Gafar, "Estimation of specific surface area using Langmuir isotherm method," *Journal of Applied Sciences and Environmental Management*, vol. 14, no. 4, pp. 1–5, 2011.

[42] D. Zohreh and F. Abedi, "Efficacy of impregnated active carbon in manganese removal from aqueous solutions," *Journal of Advances in Environmental Health Research*, vol. 7, pp. 113–121, 2019.

[43] P. Rose, S. Hager, K. Glas, D. Rehmann, and T. Hofmann, "Coating techniques for glass beads as filter media for removal of manganese from water," *Water Science and Technology: Water Supply*, vol. 17, no. 1, pp. 95–106, 2017.

[44] R. Dubey, D. S. Bag, V. K. Varadan, D. Lal, and G. N. Mathur, "Polyaniline coating on glass and PMMA microspheres," *Reactive and Functional Polymers*, vol. 66, no. 4, pp. 441–445, 2006.

[45] ICCD, "The International Centre for Diffraction Data," 2012, 2020, http://www.icdd.com.

[46] G. K. Khadse, P. M. Patni, and P. K. Labhasetwar, "Removal of iron and manganese from drinking water supply," *Sustainable Water Resources Management*, vol. 1, no. 2, pp. 157–165, 2006.

[47] O. F. Okeola, E. O. Odebunmi, O. M. Ameen, and G. B. Adebayo, *Adsorption of iron (III) ion from aqueous solution using Jatropha adsorption of iron (III) ion from aqueous solution using Jatropha curcas seed coat activated carbon*, KWA, Chemistry Department, University of Ilorin, Ilorin, Nigeria, 2011.

[48] M. A. Al-Ghouti and D. A. Da'ana, "Guidelines for the use and interpretation of adsorption isotherm models: a review," *Journal of Hazardous Materials*, vol. 393, Article ID 122383, 2020.

[49] X. Chen, "Modeling of experimental adsorption isotherm data," *Information*, vol. 6, no. 1, pp. 14–22, 2015.

[50] K. Y. Foo and B. H. Hameed, "Insights into the modeling of adsorption isotherm systems," *Chemical Engineering Journal*, vol. 156, no. 1, pp. 2–10, 2010.

[51] A. Gholizadeh, M. Kermani, M. Gholami, and M. Farzadkia, "Kinetic and isotherm studies of adsorption and biosorption processes in the removal of phenolic compounds from aqueous solutions: comparative study," *Journal of Environmental Health Science and Engineering*, vol. 11, no. 1, pp. 1–10, 2013.

[52] H. M. F. Freundlich, "Over the adsorption in solution," *Journal of Physical Chemistry*, vol. 57, pp. 385–471, 1906.